Plasmon dynamics in strongly driven finite few-electron quantum systems: The role of the surface

Carlos F. Destefani,* Chris McDonald,† Suren Sukiasyan, and Thomas Brabec
Physics Department and Center for Photonics Research, University of Ottawa, Ottawa, Canada ON K1N6N5
(Received 26 November 2009; published 19 January 2010)

An *ab initio* analysis of laser driven, few-electron plasmon dynamics in a finite lateral quantum dot is performed. The results are analyzed by a comparison to a Drude model based on the center-of-mass motion of the plasmon. We find that decay and energy absorption during the plasmon-surface interaction do not depend on electron correlation. This suggests that the Kohn theorem—plasmon dynamics in infinite parabolic quantum dots does not depend on electron correlation—is extendable to finite quantum dots.

DOI: 10.1103/PhysRevB.81.045314 PACS number(s): 73.21.La, 71.10.−w, 72.20.Ht

I. INTRODUCTION

Many-body physics in infinite systems is relatively well understood. Much progress has been made lately in the analysis and understanding of finite many-body quantum systems via approaches such as configuration interaction,[1–3] Monte Carlo,[4,5] and unrestricted Hartree-Fock.[6–8] However, most of these static theoretical methods work well only for the calculation of the ground and first few excited states. In terms of dynamics, this means that only weakly perturbed systems can be calculated.[9] Due to the lack of theoretical tools not much is known about strongly driven finite many-particle quantum systems.

This paper presents a first step toward closing this gap. The recent development of the multiconfiguration time-dependent Hartree-Fock (MCTDHF) method[10–13] allows the investigation of the dynamics of strongly driven few-body quantum systems, fully accounting for electron correlation. We focus on the investigation of the dynamics in a resonantly driven few-electron, lateral parabolic quantum dot (QD). More specifically, we solve the Schrödinger equation for four electrons with two spatial dimensions per electron (4×2D) for a broad range of QD sizes and therewith electron correlations, covering the phase transition from an electron liquid[14] to a Wigner crystal.[15]

In an infinite parabolic QD, with confining frequency ω_0, radiation only couples to the center of mass of the multielectron system,[16,17] which moves collectively as a plasmon with frequency $\omega_p=\omega_0$ (Kohn mode). In the presence of a surface, ionization and dissipation and dephasing of the plasmon dynamics take place. The goal of our investigation is to understand and characterize these surface effects as a function of electron correlation and electric field strength. The relevance of our investigation is not confined to QDs, but relates to all finite quantum systems with collective plasmonlike response, such as clusters nanoparticles, large molecules, and harmonic traps. Our proof-of-principle *ab initio* calculation of this ubiquitous process presents the first main result of this paper.

A comparison between a Drude model[18] and *ab initio* results is used to analyze the plasmon dynamics in a finite QD. This comparison reveals the second main result of our work. The Kohn theorem states that the plasmon motion in an infinite QD does not depend on electron correlation. We find that energy absorption and dissipation of the plasmon do not depend on electron correlation either. This numerical evidence suggests that the Kohn theorem is extendable from infinite to finite QDs. The corroboration of our result for larger numbers of electrons requires further tuning and optimization of MCTDHF, which is subject to future research.

Finally, the Drude model works well even in the nonperturbative limit of plasmon-surface interaction, where substantial ionization takes place. Ionization sets a limit to the ultimate field strengths the QD can be exposed to. A simple picture for the ionization process is developed, from which ionization saturation field strengths can be determined.

II. THEORETICAL APPROACH

The few-electron dynamics in the QD is described by the Schrödinger equation in effective atomic units

$$i\frac{\partial}{\partial t}\Psi = H\Psi = \left[\sum_{i=1}^{f} H_1(\mathbf{r}_i,t) + \sum_{i=1}^{f}\sum_{j>i}^{f} H_2(\mathbf{r}_i,\mathbf{r}_j)\right]\Psi, \quad (1)$$

where $\mathbf{r}=(x,y)$ is the two-dimensional (2D) vector, $f=4$ is the number of electrons in the present work, and the in-plane 4×2D wave function is $\Psi=\Psi(\mathbf{r}_1,\ldots,\mathbf{r}_f;t)\otimes\Upsilon(\mathbf{s}_1,\ldots,\mathbf{s}_f)$. Here, Υ labels the spin part of the wave function with $\mathbf{s}$ the spinors. The spin state Υ remains conserved during the dipole light-QD interaction investigated here. The one-electron Hamiltonian is $H_1=T+V(\mathbf{r})+\mathbf{F}(t).\mathbf{r}$, with $T=-\nabla^2/2$ the kinetic-energy operator, and $\mathbf{F}(t).\mathbf{r}$ the electron-laser interaction term in dipole approximation and in length gauge. The finite QD parabolic confinement is $V(\mathbf{r})=-\omega_0^2(r_c^2-r^2)\Theta(r_c-r)/2$, where Θ is a step function and ω_0 the confining frequency; the QD boundaries are at $r_c=\sqrt{x_c^2+y_c^2}$, so that V is nonzero only for $r\leq r_c$ [see one-dimensional (1D) profile in inset of Fig. 1(d)]. The depth of the QD is given by $V_{min}=-\omega_0^2 r_c^2/2$, and the number of single-electron bound states contained in the finite QD is given by $s=V_{min}/\omega_0$. The small fluctuations of V due to the host matrix are neglected here, as our emphasis is on the investigation of surface effects. The two-electron Hamiltonian is $H_2=1/\sqrt{(\mathbf{r}_2-\mathbf{r}_1)^2+a^2}$ with the parameter a arising from the finite thickness of the 2D QD. Effective atomic units are used throughout the paper, which for a GaAs QD with effective mass $m=0.067$ and dielectric constant $\epsilon=12.4$ reads $R^*=9.80$ nm (Bohr radius), $E^*=11.85$ meV

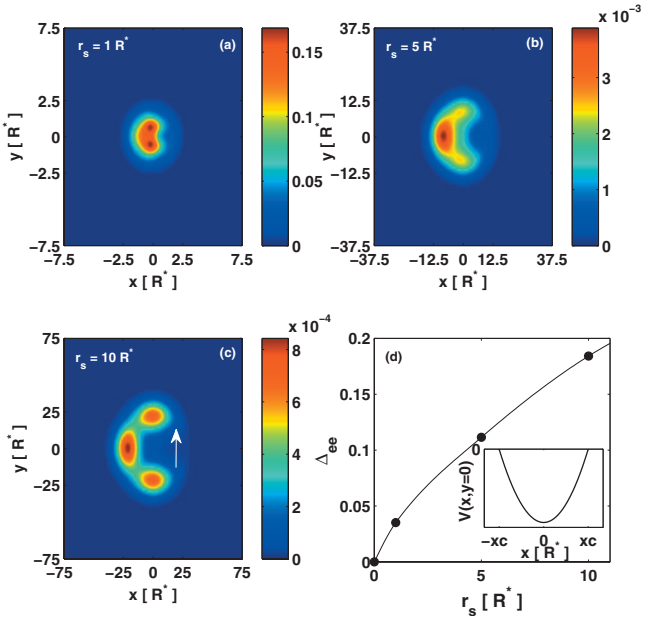

FIG. 1. (Color) Ground-state conditional probability distribution, $P_c(\mathbf{r},t=0)$, for the three-electron correlation r_s values considered in our work, as given by MCTDHF: $r_s=1R^*$ [liquid phase, (a)], $r_s=5R^*$ (b), and $r_s=10R^*$ [solid phase, (c)]; R^* is the effective atomic length unit. The limits of the plot range in each panel are equal to the extension of the finite parabolic potential, r_c, whose 1D profile is shown in inset in (d). The parameters r_s and r_c are changed in a way leaving $s=\omega_0 r_c^2/2=$const. The full simulation box is five times larger than (x_c,y_c) to capture all of the electron dynamics. (d) shows the normalized correlation energy, Δ_{ee}, as a function of the electron correlation parameter r_s. In all panels, $\int d\mathbf{r} P_c(\mathbf{r},t=0)=1$.

(Hartree energy), $T^*=55.55$ fs (natural time), and $F^*=1.21\times10^4$ V/cm (electric field).

Equation (1) is solved by the MCTDHF approach, which relies on the ansatz

$$\Psi(\mathbf{r}_1,\ldots,\mathbf{r}_f;t)=\sum_{j_1\cdots j_f=1}^{n} A_{j_1\cdots j_f}(t)\phi_{j_1}(\mathbf{x}_1,t)\ldots\phi_{j_f}(\mathbf{x}_f,t), \tag{2}$$

where $\mathbf{x}_i=(\mathbf{r}_i,\mathbf{s}_i)$. Both, $A_{j_1\cdots j_f}(t)$ and $\phi_j(\mathbf{x},t)$ are time dependent and are determined variationally. For further details, see Refs. 10–13. The initial ground state at $t=0$ is obtained via imaginary time propagation. A basis set with $n=30$, yielding $\approx3\times10^5$ configurations was found sufficient for convergence. The size of the simulation boxes is $5\mathbf{r_c}$ and 512 points per dimension are used. Although the number of orbitals $n=30$ was kept constant in all our simulations, we would like to note that in the weakly correlated, low-field limit $n=20$ would be sufficient.

The laser-driven QD dynamics is investigated as a function of the electron correlation, $r_s=[e^2/(\varepsilon l_0)]/(\hbar\omega_0)$, which is the ratio of electron-electron interaction energy to kinetic energy. In effective units, $r_s=l_0$, with $l_0=1/\sqrt{\omega_0}$ the radius of the QD ground state. Correlation is varied in the range $r_s=1-10R^*$, which covers the transition from an electron liquid in a tightly confined QD at $r_s=1R^*$ to the initial stages of Wigner electron crystallization in a wide QD at $r_s=10R^*$. Throughout this range, the ground state is a triplet. The shielding parameter is $a=0.1r_s$.

The phase transition can be visualized by looking at the conditional probability distribution, $P_c(\mathbf{r},t)=\int d\mathbf{r}_3\int d\mathbf{r}_4|\Psi^*(\mathbf{r},\mathbf{r}_2=\mathbf{r}_a,\mathbf{r}_3,\mathbf{r}_4;t)|^2$, where one electron is fixed at a position $\mathbf{r}_a$ with a given spin. Figure 1 shows $P_c(\mathbf{r},0)$ for three distinct QD ground states, at (a) $r_s=1R^*$, (b) $5R^*$, and (c) $10R^*$, where the fixed $\uparrow$ electron at $\mathbf{r}_a$ is explicitly shown only in (c). Whereas the remaining three electrons are more uniformly distributed in the QD in the liquid phase (a), the dominant electron-electron repulsion results in crystallization and in three distinct maxima in the solid phase (c), while (b) presents an intermediary case. The ground-state energies are $E_0=-102.2856E^*$, $E_0=-3.6445E^*$, and $E_0=-0.8103E^*$ for (a), (b), and (c), respectively. In Fig. 1(d), the ratio $\Delta_{ee}=(E_0-\bar{E}_0)/|\bar{E}_0|$ is plotted as a function of r_s, where $\bar{E}_0$ is the bound-state energy in the noninteracting limit. This ratio increases almost linearly with r_s, as a result of the increasing correlation and electron repulsion.

Our study focuses on the resonant dynamics, with laser frequency $\omega_l=\omega_0=\omega_p$, where ω_p is the plasmon (Kohn) frequency of an infinite harmonic potential. The laser pulse, $F(t)=F_0\sin(\omega_0 t)f(t/\tau)$ is polarized along $\hat{x}$. The envelope is a half-cycle $\sin^2$ pulse, $f=\sin^2[\pi t/(n_c\tau)]$, which is $n_c=3$ optical cycles long; $\tau=2\pi/\omega_0$ is the optical cycle and F_0 the peak field strength. The simulation is run for another cycle after the end of the pulse, see inset of Fig. 2(c).

III. ANALYSIS OF PLASMON SURFACE DYNAMICS

In order to isolate the effect of electron correlation on the plasmon dynamics in a finite QD, care has to be taken with the variation in the parameters. A change in the electron correlation, $r_s=1/\sqrt{\omega_0}$, also changes the single-electron properties of the QD, which is undesirable. Therefore, to isolate the role of correlation, both QD parameters r_s and r_c have to be varied in a way that the resulting changes in the single-electron properties of the QD are trivial. This can be achieved by using the transformation $T=t\omega_0$, $(\xi,\eta)=\sqrt{\omega_0}(x,y)$, and $\rho=\sqrt{\omega_0}r$, which renders the Schrödinger equation for the single-electron QD into

$$i\frac{d}{dT}\Psi=-\frac{1}{2}\left(\frac{d^2}{d\xi^2}+\frac{d^2}{d\eta^2}\right)\Psi+V(\rho)\Psi-\xi F(T)\Psi. \tag{3}$$

Here, $F(T)=F_s f(2\pi T)\sin(T)$, $F_s=F_0/\omega_0^{3/2}$, $\rho_c=\sqrt{\omega_0}r_c$, and $V=(-s+\rho^2/2)\Theta(\rho_c-\rho)$. In our simulations, see Fig. 1, r_s and r_c are changed in a way leaving the number of single-particle eigenstates contained in the QD constant, $s=\omega_0 r_c^2/2=28$. As a result, Eq. (3) becomes scaling invariant with regard to changes in ω_0 (r_s), and the surface-induced decay of the laser-driven single-electron motion is proportional to $\exp(-\gamma_0 T)$. From a solution of the single-electron Schrödinger Eq. (3) for various field strengths F_0 we obtain $\gamma_0=0.5$. Transformation back to effective units yields a decay $\exp(-\gamma t)$ with surface collision frequency $\gamma=\omega_0\gamma_0$. As a result, the decay constant measured in units of oscillation

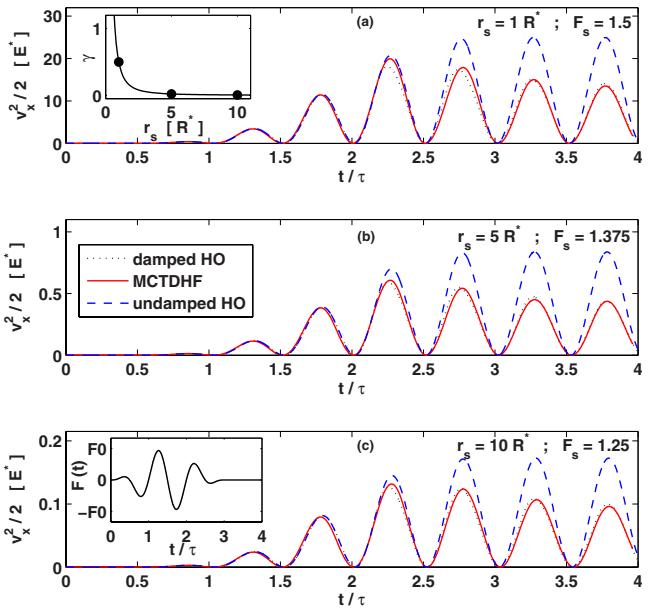

FIG. 2. (Color online) Time evolution of the kinetic energy, $v_x^2/2$, in the $\hat{x}$ direction of the external pulse $F(t)$, for each electron correlation (r_s) value considered in Fig. 1 as a function of optical cycles (t/τ). The plots are for the highest (normalized field) F_s values used in our simulation. In all panels, dashed, solid, and dotted lines, respectively, stand for undamped HO, MCTDHF, and damped HO results. The simulation time extends over the three-cycle pulse plus an extra cycle, as shown in inset in (c); τ is the laser oscillation period. Inset in (a) shows the collision frequency γ as a function of r_s. The Drude model parameters v_c and β (see text) depend smoothly on r_s and weakly on F_s. We use $v_c \approx 5.0, 0.85, 0.38$, and $\beta \approx 0.005, 0.01, 0.015$, for $r_s = 1R^*$, $5R^*$, and $10R^*$, respectively.

periods is constant, $\gamma\tau = 2\pi\gamma_0$. When the *ab initio* few-electron plasmon decay follows this relation, it can be modeled by an effective single-particle, uncorrelated, center-of-mass Hamiltonian. Any deviation from this relation must be attributed to electron correlation.

The plasmon-surface dynamics is analyzed by comparing the *ab initio* results with a classical damped harmonic oscillator (HO) Drude model,

$$\ddot{x} = F(t) - \omega_0^2 x(t) - 2\gamma\dot{x}(t), \tag{4}$$

where γ is the surface collision frequency. In order to get good agreement with the quantum results, we found that the Drude model has to be modified for surface collisions. First, in the strong field limit, the bound wave function is driven over the surface which modifies the plasmon frequency $\omega_0 = \omega_p$. This is accounted for by substituting $\omega_0^2 \to \omega_0^2(1-\beta^2)$. In a more detailed model, the frequency shift β should appear only during the times in the laser cycle where the wave function is strongly deflected by the surface. Second, surface dissipation does cutoff at a velocity v_c, below which the plasmon does not reach the surface anymore. This is accounted for by cutting dissipation for plasmon velocities $v \le v_c$. The phenomenological modifications identified here present a starting point for developing a generalized Drude model for plasmon-surface collisions, which is beyond the scope of this paper. We would like to emphasize that they are needed to obtain fair agreement with the quantum result over the whole simulation range in Fig. 2. However, they are not needed to determine γ, which can be obtained from fitting the plasmon decay in the time interval in which $v \ge v_c$.

The time evolution of the kinetic energy in $\hat{x}$ direction is shown in Fig. 2 as determined by the MCTDHF analysis (full), the classical damped HO of Eq. (4) (dotted), and the classical undamped HO model (dashed); (a), (b), and (c) show the results for $r_s = 1R^*(F_s = 1.5)$, $r_s = 5R^*(F_s = 1.375)$, and $r_s = 10R^*(F_s = 1.25)$, respectively. The MCTDHF plasmon expectation values are calculated by using the part of the wave function in the box circumscribing the QD; as for some of the parameters substantial ionization takes place, the total wave function has to be split into a plasmonic, bound part and an ionized part.

The main result obtained from the Drude model fit is the relation for the collision frequency, $\gamma = \omega_0/2 = 1/(2r_s^2)$, see inset of Fig. 2(a). We have performed many more calculations in the parameter range $r_s = 1-10R^*$ and $F_s = 0.5-1.5$. In the whole range, γ is independent of F_s. The ω_0 dependence of γ is identical with the scaling in the single-electron limit, derived above. As a result, the influence of correlation on the surface-induced plasmon decay is negligible. In terms of the energy spectrum, surface dissipation comes from a coupling between plasmon and highly excited electronic states, close to the continuum threshold.

In Fig. 2 the highest field dynamics are displayed, to demonstrate that the Drude model works well even in the nonperturbative limit, where substantial ionization takes place, see Fig. 4. All fits, in the whole simulation range defined above, show an agreement comparable to or better than the ones in Fig. 2. At weaker fields, not shown here, where the interaction with the surface is negligible, the classical undamped model reproduces exactly the MCTDHF result, in agreement with the Kohn theorem.

Besides dephasing the plasmonic motion, the surface also modifies the energy absorption process. In Fig. 3 the total energy absorbed during the QD-laser interaction, $E_{abs} = \int_0^{4\tau} dt' \Sigma_{i=1}^{f} F_i(t') \langle \Psi(t') | \mathbf{v}_i | \Psi(t') \rangle$, is plotted versus F_s. Integration is again performed over the box circumscribing the QD. In the classical analysis $\langle \Psi(t') | \mathbf{v}_i | \Psi(t') \rangle$ is replaced by $\dot{x}_i(t)$ from Eq. (4). We have plotted $E_{abs}/|E_0|$, the absorbed energy over the ground-state binding energy, for $r_s = 1R^*$, $5R^*$, and $10R^*$.

Figure 3 shows that even at high F_s values, the influence of the surface is weak and energy absorption is always dominated by the plasmon resonance. As a result, both, plasmon dissipation and energy absorption in the presence of a surface do not depend on electron correlation. Note that the highest F_s values used here at each r_s are the highest values that can be applied to the neutral QD; as ionization of the first electron is already substantial, higher values of F_s would lead to its complete ionization, see Fig. 4.

IV. PLASMON-ASSISTED SINGLE AND DOUBLE IONIZATION

Plasmon-assisted ionization can be understood in terms of a simple picture. The ionization potential of the weakest

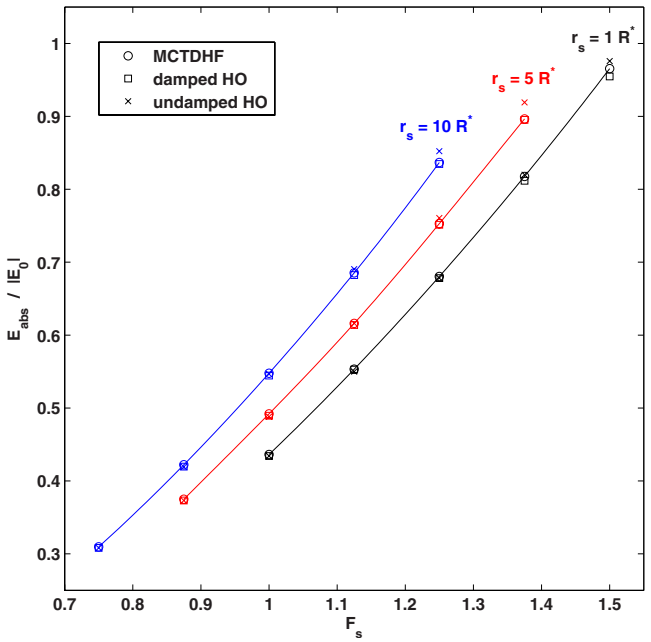

FIG. 3. (Color online) Total absorbed energy scaled by (four-electron) QD ground-state energy, $E_{abs}/|E_0|$, as a function of unitless field strength F_s at the end of the laser pulse for $r_s=1R^*$, $5R^*$, and $10R^*$; quantum MCTDHF (circles), classical damped HO (squares), and classical undamped HO (crosses) calculations.

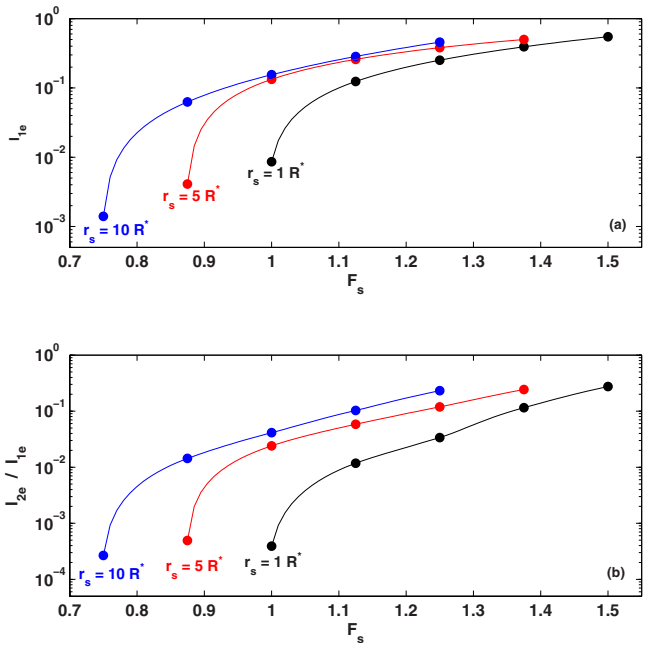

FIG. 4. (Color online) MCTDHF results for ionization probability at the end of the laser pulse for $r_s=1R^*$, $5R^*$, and $10R^*$, as a function of normalized field strength F_s. (a) One-electron ionization probability, I_{1e}; (b) ratio of two-electron ionization to one-electron ionization probability, I_{2e}/I_{1e}.

bound electron is given by I_p, which denotes the energy required to remove it from the QD. As the plasmon dynamics is a collective effect, each of the electrons carries on average the same amount of energy, $E_{abs}/4$. When $E_{abs}/4=I_p$, the weakest bound electron has absorbed sufficient energy to leave the QD by above barrier ionization. Around the onset of above barrier ionziation the probability of ionization of the weakest bound electron approaches unity and ionization saturates.

This picture is quantitatively corroborated by Fig. 4(a), where the one-electron ionization probability, I_{1e}, is shown versus F_s. The values of I_p are $24.66E^*$, $0.76E^*$, and $0.14E^*$ for $r_s=1R^*$, $5R^*$, and $10R^*$, respectively. Using Fig. 3 we find the F_s values at which $E_{abs}/4=I_p$ to be, respectively, 1.49, 1.32, and 1.14. At these F_s values, close to 50% of the first electron has been ionized, i.e., ionization is starting to saturate, in agreement with the picture developed above. These F_s values present the saturation field strengths for one-electron ionization, which is the ultimate field strength the (neutral) QD can be exposed to.

As the plasmon oscillation is a collective motion and the gained energy is shared between the electrons, not only the ionization of the first electron is accelerated but also correlated tunnel ionization of two or more electrons can take place. The ratio of one-electron to two-electron ionization probability, I_{2e}/I_{1e}, is shown in Fig. 4(b). Whereas at small F_s this ratio is small, $I_{2e}/I_{1e}\simeq 0.25$ becomes substantial for the highest F_s values at each correlation r_s.

V. CONCLUSION

An *ab initio* analysis of a laser-driven plasmon in a finite lateral quantum dot was performed for the special case of four electrons. The correlation of the electrons was tuned from the weakly correlated with strongly correlated limit of Wigner crystallization. We have found that the influence of correlation on the surface-induced plasmon decay is negligible. This suggests that the Kohn theorem—plasmon dynamics in infinite parabolic quantum dots does not depend on electron correlation—is extendable to finite quantum dots, which will have to be corroborated by calculations with a larger number of electrons.

*carlos.destefani@uottawa.ca
†cmcdo059@uottawa.ca

[1] M. Rontani, C. Cavazzoni, D. Belluci, and G. Goldoni, J. Chem. Phys. **124**, 124102 (2006).
[2] R. M. Abolfath and P. Hawrylak, J. Chem. Phys. **125**, 034707 (2006).
[3] M. Koskinen, M. Manninen, and P. O. Lipas, Phys. Rev. B **49**, 8418 (1994).
[4] A. V. Filinov, M. Bonitz, and Y. E. Lozovik, Phys. Rev. Lett. **86**, 3851 (2001).
[5] A. D. Güçlü, A. Ghosal, C. J. Umrigar, and H. U. Baranger, Phys. Rev. B **77**, 041301(R) (2008).

[6] U. De Giovannini, F. Cavaliere, R. Cenni, M. Sassetti, and B. Kramer, Phys. Rev. B **77**, 035325 (2008).
[7] B. Reusch and H. Grabert, Phys. Rev. B **68**, 045309 (2003).
[8] C. Yannouleas and U. Landman, Phys. Rev. B **68**, 035325 (2003).
[9] M. Brack, Rev. Mod. Phys. **65**, 677 (1993); E. A. Jagla, K. Hallberg, and C. A. Balseiro, Phys. Rev. B **47**, 5849 (1993).
[10] C. F. Destefani, C. McDonald, S. Sukiasyan, and T. Brabec, Phys. Rev. B **79**, 155322 (2009).
[11] C. F. Destefani, C. McDonald, R. M. Abolfath, P. Hawrylak, and T. Brabec, Phys. Rev. B **78**, 165331 (2008).
[12] J. Caillat, J. Zanghellini, M. Kitzler, O. Koch, W. Kreuzer, and A. Scrinzi, Phys. Rev. A **71**, 012712 (2005).
[13] J. Zanghellini, M. Kitzler, T. Brabec, and A. Scrinzi, J. Phys. B **37**, 763 (2004).
[14] M. Santer, B. Mehlig, and M. Moseler, Phys. Rev. Lett. **89**, 286801 (2002).
[15] S. Kalliakos, M. Rontani, V. Pellegrini, C. P. García, A. Pinczuk, G. Goldoni, E. Molinari, L. N. Pfeiffer, and K. W. West, Nat. Phys. **4**, 467 (2008).
[16] P. A. Maksym and T. Chakraborty, Phys. Rev. Lett. **65**, 108 (1990).
[17] P. Hawrylak, P. A. Schulz, and J. J. Palacios, Solid State Commun. **93**, 909 (1995).
[18] H. Reinholz, R. Redmer, G. Röpke, and A. Wierling, Phys. Rev. E **62**, 5648 (2000).